Interpretation of Dauphiné-twin-domain configurations resulting from the α-β phase transition in quartz and aluminum phosphate

J. Van Landuyt, G. Van Tendeloo, and S. Amelinckx*
University of Antwerp Rijksuniversitair Centrum Antwerpen, Groenenborgerlaan 171, B-2020 Antwerpen, Belgium

M. B. Walker
Department of Physics and Scarborough College, University of Toronto, Toronto, Ontario, Canada M5S 1A7
(Received 28 September 1984)

Electron microscope observations of domain configurations associated with the incommensurate phases of quartz and aluminum phosphate are presented and successfully interpreted in terms of a theoretical model.

Van Tendeloo *et al.*[1,2] have observed, by dark-field-imaging electron microscopy, an incommensurate triangular domain structure in a narrow temperature interval between the high-temperature β phase and the low-temperature α phase in both quartz and aluminum phosphate; a wide variety of irregular domain configurations were also observed. More recent electron microscopy[3] and neutron scattering[3,4] studies have further enhanced our knowledge of these structures. A theoretical model which could possibly account for such a wide variety of domain configurations has been developed by Walker.[5] The purpose of the present article is to make as detailed a comparison of the predictions of the model with the electron microscope observations as possible; the result of this examination will be the conclusion that the essential regularities of the observed domain structures can be well understood in terms of the model.

The phase transition from the β phase to the α phase of quartz is a structural phase transition, as a result of which the ions undergo displacements, as shown in Fig. 1 (Ref. 6). A similar transition occurs in aluminum phosphate.[6] The order parameter η for the phase transition can be taken to have a magnitude equal to the magnitude of the displacement of a given silicon ion, and is positive if the displacement is in the direction indicated and negative if the displacement is in the opposite direction. The order parameter is zero in the β phase and increases in magnitude as the temperature is lowered into the α phase.[7] The so-called Dauphiné twin domains, which appear as dark or bright domains in the electron micrographs, correspond to the fact that η can be either positive or negative. That the two Dauphiné twin domains have the same free energy follows from the symmetry of quartz.

The original electron microscope studies,[1,2] in addition to revealing the fascinating microdomain structure exhibited by quartz and aluminum phosphate, found that the walls of the domains were approximately parallel to $(10\bar{1}0)$ planes of the structure, i.e., parallel to the plane containing both the **c** axis and the **x** axis of Fig. 1. This is consistent with more recent neutron scattering work[3,4] which found the incommensurate wave vectors to be parallel to the **y** axis of Fig. 1, or its equivalent, to within experimental error.

A theoretical calculation[5] of the free energy of a domain wall as a function of its orientation has, however, established that the domain walls cannot be exactly parallel to the **x** axis. Because this result is central to the understanding of the domain structure of quartz, we will begin by giving a derivation of it. The present derivation is more general than the previous one since it follows from symmetry considerations only, and is independent of the detailed form of an assumed model free energy. In a complementary study, Aslanyan *et al.*[8] have found that the incommensurate wave vectors are rotated away from the high-symmetry directions, a result closely related to the domain-wall orientation results of Ref. 5.

Domain walls of three different orientations are shown schematically in Fig. 2. In order to simplify this figure, only the displacements of the silicon ions labeled 1 in Fig. 1 have been included whereas those of the ions labeled 2 and 3 have been omitted. In Fig. 2(a), the domain wall is

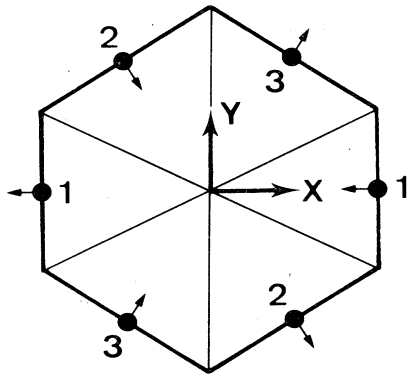

FIG. 1. Basal-plane projection of the position of the silicon ions in the Wigner-Seitz cell of the quartz structures. The solid circles give the silicon positions in the β phase, whereas the arrows give the directions of the silicon displacements in the transition to the α phase. The direction of the **x** axis is also defined by this figure. Aluminum phosphate is described by an identical figure, except that a point representing the basal-plane projection of a column of silicon ions must be interpreted as representing the basal-plane projection of a column of alternating aluminum and phosphorus ions.

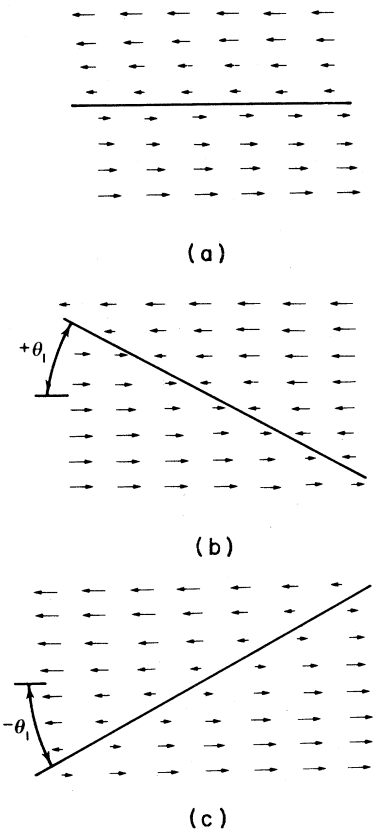

FIG. 2. Domain walls of three different orientations. Each wall separates a Dauphiné twin corresponding to $\eta=+\eta_0$ in the upper part of the figure from a twin corresponding to $\eta=-\eta_0$ in the lower part. The displacements of the silicon ions labeled 1 in Fig. 1 are indicated by the arrows in the figure and are parallel to the **x** axis of Fig. 1; the displacements of the ions labeled 2 and 3 in Fig. 1 have been omitted for simplicity. The center of a domain wall is indicated by a solid line.

parallel to the **x** axis of Fig. 1. In Fig. 2(b) the domain wall has been rotated (about the **c** axis) by the angle θ, in what we define to be the positive sense; the silicon-ion displacements shown in this figure are toward the solid line defining the wall center, and this wall will therefore be called a heavy wall. It can be seen in Fig. 2(c) that a rotation of the wall in the negative direction results in a situation where the silicon displacements are away from the solid line marking the center of the wall, and this wall will therefore be called a light wall.

Two possibilities for the free energy per unit area $F(\theta)$ of the wall as a function of the angle θ are shown in Fig. 3. In (a) the free energy is the same for orientations $+\theta_1$ and $-\theta_1$, whereas in (b), this is not the case. Since it has just been shown for the domain walls in quartz that rotations by $+\theta_1$ and $-\theta_1$ produce physically inequivalent states (corresponding to heavy walls and light walls, respectively), the curve of Fig. 3(a) will not in general be applicable, and the appropriate curve for our case is that of Fig. 3(b). The equilibrium orientation of a domain wall [found by minimizing $F(\theta)$] is therefore not exactly

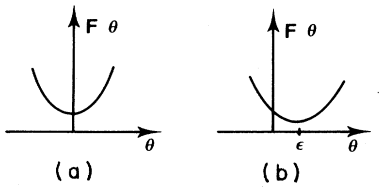

FIG. 3. Two possibilities for the free energy per unit area of a domain wall as a function of its orientation.

parallel to the **x** axis, in agreement with the previous discussion.[5] Another way of arriving at this result is to consider the expansion of the free energy per unit length $F(\theta)$ in powers of θ, i.e.,

$$F(\theta)=f_0(T,P)+f_1(T,P)\theta+\cdots ,$$

where the dependence of the coefficients f_0 and f_1 on temperature T and pressure P is shown explicitly. Since the coefficient $f_1(T,P)$ of the term linear in θ is not required to be zero by symmetry, it will not in general be zero (although it may become zero at some particular temperature and pressure); thus, in general, Fig. 3(b), which shows the influence of a nonzero term linear in θ, is applicable.

According to Walker's analysis of a phenomenological model[5] the equilibrium orientation of a wall is obtained for θ having the value ϵ where

$$\epsilon=C\frac{\int(d\eta/dx')^3dx'}{\int(d\eta/dx')^2dx'} .$$

Here η is the order parameter defined above in connection with the discussion of Fig. 1, the coordinate x' is measured normal to the wall, and C is a constant. The order parameter is expected to be constant except in the neighborhood of the domain wall where it varies from $-\eta_0$ on one side of the wall to $+\eta_0$ on the other side of the wall, indicating a transition between two Dauphiné twins. If the width of this transition region is w, ϵ can be roughly evaluated as

$$\epsilon\simeq C'\eta_0/w$$

where C' is a new constant. This formula shows that as the temperature is lowered from the β phase to the incommensurate phase transition temperature, ϵ is expected to increase since η_0 increases and the walls are expected to sharpen up. This qualitative behavior is consistent with the results on rotation obtained in Ref. 8 from a different point of view. Experimental evidence for the increase of ϵ as well as for the decrease in domain-boundary width with decreasing temperature will be presented below.

So far it has been assumed that the domain walls are parallel to the **c** axis. To see if this configuration can be a stable one, consider a domain wall W which contains the **c** axis and let the line of intersection of the wall W with the basal plane be called the **x'** axis. Also consider the walls W' and W'' obtained by rotating W about the **x'** axis by the small angles $+\phi$ and $-\phi$, respectively. Now note that a rotation of the crystal by an angle π about the

c axis does not change the energy of the crystal but converts the wall W' into the wall W''. Therefore, the energy of the wall is an even function of the angle ϕ and in particular is forbidden by symmetry to contain a term linear in ϕ. It is therefore consistent with the symmetry of quartz to have domain walls which are parallel to the c axis and which are stable with respect to the small rotations about the x′ axis just considered.

Now suppose that the equilibrium orientation of a domain wall has been found, and suppose that it is as shown in Fig. 2(b). This domain wall is shown again in Fig. 4(a) (it is the wall which is the farthest to the right of the three shown). It follows from the symmetry of quartz that five other walls have the same free energy as this one, and all six of these walls are shown in (a) and (b) of Fig. 4. The walls called θ_+ walls make angles of $+\epsilon+2\pi n/3$ with the x axis ($n=-1,\ 0,\ +1$) and are shown in Fig. 4(a), whereas the walls called θ_- walls make angles $-\epsilon+2\pi n/3$ ($n=-1,\ 0,\ +1$) with the x axis. A number of possible ways in which domain walls may intersect are also shown in Fig. 4; we refer to Ref. 5 for more detailed discussion of the various possible domain-wall intersections. It is important to note that the angles at which the walls intersect are all determined in terms of a single parameter, namely ϵ, a fact which allows a qualitative test of the model. In particular, two walls can intersect only at angles of 2ϵ, 60°, $120°-2\epsilon$, and $120°+2\epsilon$.

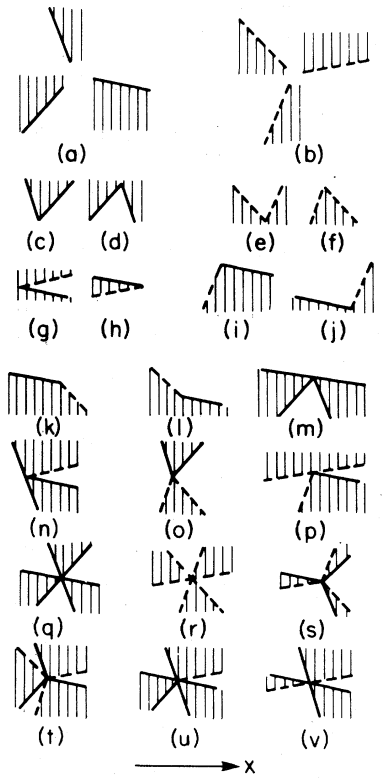

FIG. 4. Three θ_+ domain walls are shown in (a) and the θ_- domain walls are shown in (b); the shaded and unshaded regions on either side of a domain wall correspond to $\eta=-\eta_0$ and $\eta=+\eta_0$, respectively. Parts (c)—(l) show two-wall intersections; the angles of intersection of the walls are (c), $\pi/3$; (d), $\pi/3$; (e), $\pi/3$; (f), $\pi/3$; (g), 2ϵ; (h), 2ϵ; (i), $-2\epsilon+2\pi/3$; (j), $-2\epsilon+2\pi/3$; (k), $2\epsilon+2\pi/3$; (l), $+2\epsilon+2\pi/3$. Four-wall intersections are shown in (m)—(p), and six-wall intersections are shown in (q)—(v). The direction of the axis, as defined in Fig. 1, is shown at the bottom.

The original electron microscope observations[1,2] found that a relatively large scale domain structure, which was called a coarse domain structure, existed in the α phase of both quartz and aluminum phosphate [e.g., see Figs. 5 and 6—Figs. 5(a) and 6(a) have been taken from Ref. 2]. This is perhaps the best place to begin a detailed comparison of the theoretical model with the experimental results, because the relatively large scale domains and the relatively sharp domain walls allow a reasonably accurate determination of the domain-wall intersection angles. It should be noted, however, that the accuracy with which the domain-wall intersection angles can be measured is hampered by two factors. First, the domain walls are vibrating and have a certain temperature-related width on the photographs as a result of this. Second, in the dark-field-imaging technique, used for optimal structure-factor contrast, the specimen is tilted away from the c axis orientation by about 13°; as a consequence, the measured angle is a projected angle which is only approximately equal to the domain-wall intersection angle.

Now note that in the coarse domain structure of quartz shown in Fig. 5, there are only two distinct domain-wall intersection angles, namely $\lambda=101°$ and $\mu=139°$. These can be written in the form $\lambda=120°-2\epsilon$ and $\mu=120°+2\epsilon$, where 2ϵ is approximately 19°. Also, in the coarse domain structure of aluminum phosphate shown in Fig. 6, nearly all the domain-wall intersection angles are either approximately $\lambda=110°$ or $\mu=130°$. These two angles can be written in the form $120°\pm2\epsilon$, where 2ϵ is approximately 10°. Thus, already one has a good test of the model since, in each of the above examples, one has two distinct angles determined in terms of the single parameter 2ϵ.

Notice however that the angles $\lambda'=100°$ in Fig. 6(b) are approximately 10° smaller than they should be on the basis of the theoretical model, whereas the angles $\mu'=135°$ are approximately 5° too large (on the basis of the model, we should have $\lambda=\lambda'$ and $\mu=\mu'$). Furthermore, one might ask why only the intersection angles $120°\pm2\epsilon$ occur in Figs. 5 and 6, and not the intersection angles 60° and 2ϵ. In attempting to address these two problems, it is essential to appreciate that the domain walls in the α phase have a positive free energy per unit area. The incommensurate phase consists of a triangular columnar domain structure. In this phase the domain-wall energy must be assumed to be negative so that the overall free energy is lowered by packing a relatively large domain-wall surface area into the quartz crystal. If one lowers the temperature sufficiently, the domain walls remove themselves from the sample (indicating that at this temperature the walls now have positive energy) and a transition to the α phase occurs. It appears that not all of the walls are able to remove themselves from the sample, however, presumably because their motion is constrained by some unknown pinning mechanism. The walls which are left give the coarse domain structure shown in Figs. 5 and 6.

It can now be seen why only the intersection angles

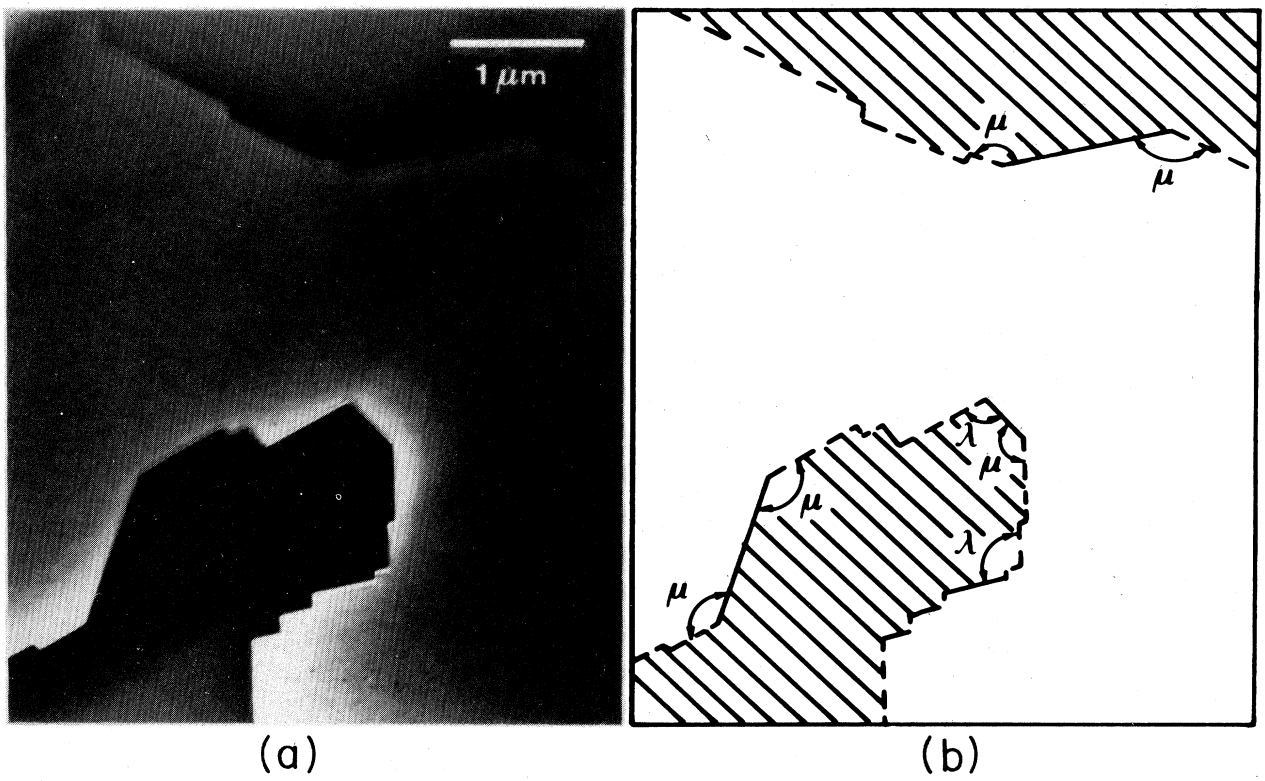

FIG. 5. (a) Dark-field image of coarse Dauphiné twins at room temperature in a foil of quartz, cut perpendicular to the **c** axis. (b) Analysis of the coarse domains of (a) in terms of the θ_+ and θ_- domain walls of Figs. 4(a) and 4(b); all of the labeled angles were measured, with the results $\lambda \simeq 101°$ and $\mu \simeq 139°$

$120° \pm 2\epsilon$ occur in the α-phase coarse domain structure. As an example, consider Fig. 7 which shows two possible ways of connecting points A and B by domain walls. Since the free energy per unit length of a domain wall in the α phase is positive, the configuration of Fig. 7(a) will be favored relative to the configuration of Fig. 7(b) because the length of wall connecting A to B in (a) is shorter than the length of wall connecting A to B in (b). In general, a shorter wall between two given points can be formed by keeping the wall intersection angles relatively large (i.e., $120° \pm 2\epsilon$) rather than by allowing them to be relatively small (i.e., 60° or 2ϵ).

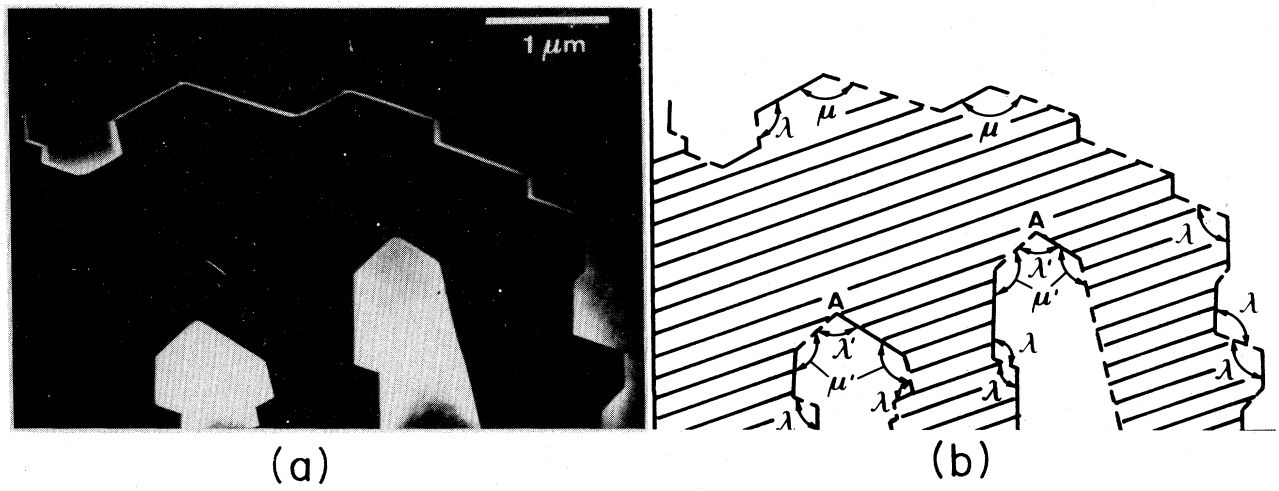

FIG. 6. (a) Dark-field image of coarse Dauphiné twins at room temperature in a foil of aluminum phosphate cut perpendicular to the **c** axis. (b) Analysis of the coarse domains of (a) in terms of the θ_+ and θ_- domain walls of Figs. 4(a) and 4(b); all of the labeled angles were measured, with the results $\lambda \simeq 110°$, $\mu \simeq 130°$, $\lambda' \simeq 100°$, and $\mu' \simeq 135°$.

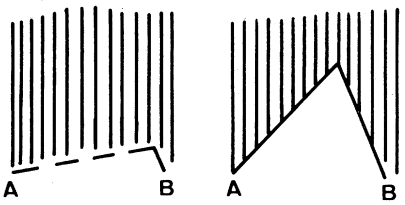

FIG. 7. Two possible ways of connecting point A to point B by domain walls selected from Figs. 4(a) and 4(b).

Suppose that we were able to somehow forcibly move the domain-wall vertices, labeled A in Fig. 6(b), a small distance towards the upper left-hand corner of the figure. This would cause an increase in the overall domain-wall length and would thus increase the free energy of the system. The force F required to bring about a quasistatic displacement dx is given by $F\,dx = df$, where df is the increase in the overall free energy. Thus, it is clear that a pinning force of magnitude F provided by some unknown mechanism is pinning the domain walls at the vertex A. Such a force would cause the domain walls to deviate somewhat from their equilibrium orientations and would result in the inequalities $\lambda' < \lambda$ and $\mu' > \mu$ which are observed. Without further quantitative work, this explanation must be regarded as being speculative, but it does have the virtue of predicting the correct signs of the angular distortions.

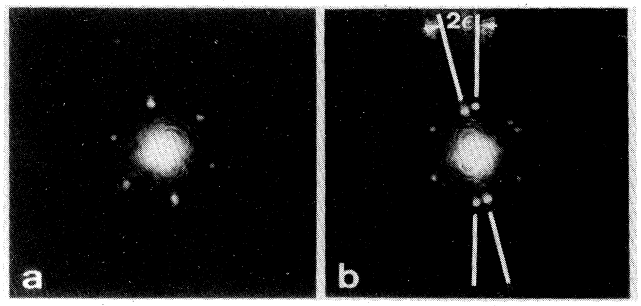

FIG. 9. Optical diffractographs of micrographs containing periodic arrays of Dauphiné twin columns. (a) Single macrodomain; (b) satellite splitting if area selected is across two macrodomains.

Figure 8 shows the triangular domain structure characteristic of the incommensurate phase. The theoretical model allows two distinct triangular domain structures to

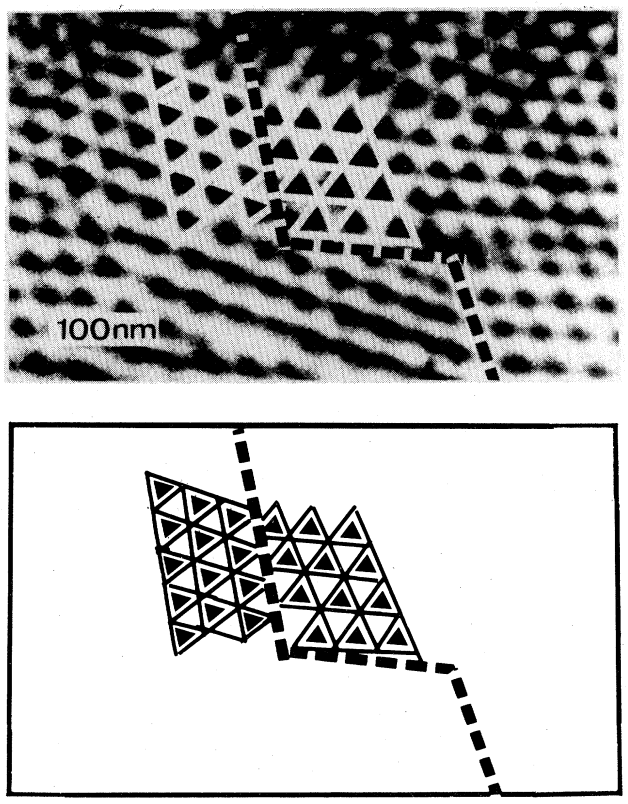

FIG. 8. An example of the triangular domain structure in quartz at a temperature of approximately $T = 846$ K showing two differently oriented macrodomains.

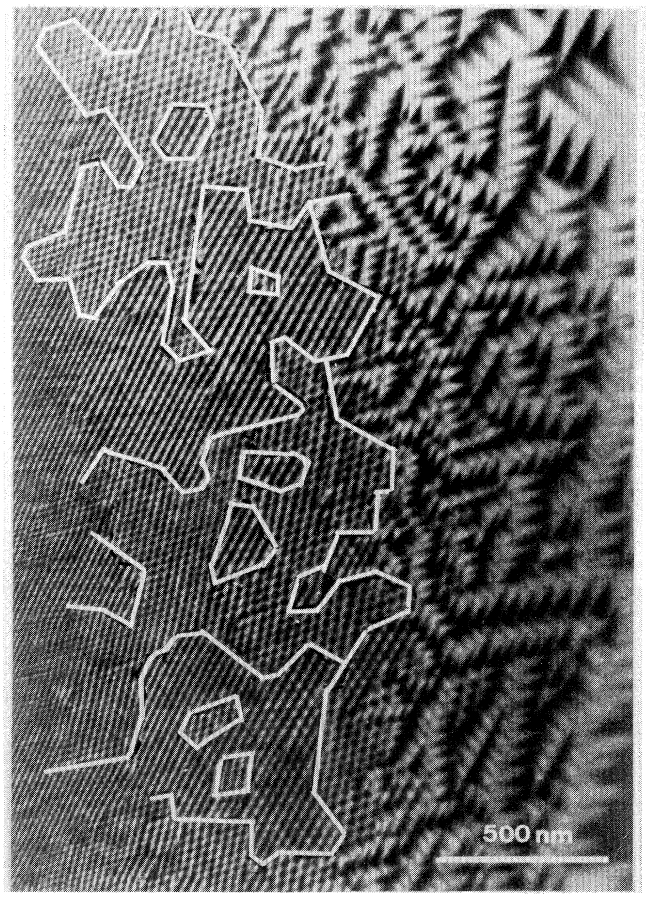

FIG. 10. Domain configuration obtained on heating from the α phase to the α-β transition temperature. A temperature gradient exists across the sample with the left of the figure being warmer than the right.

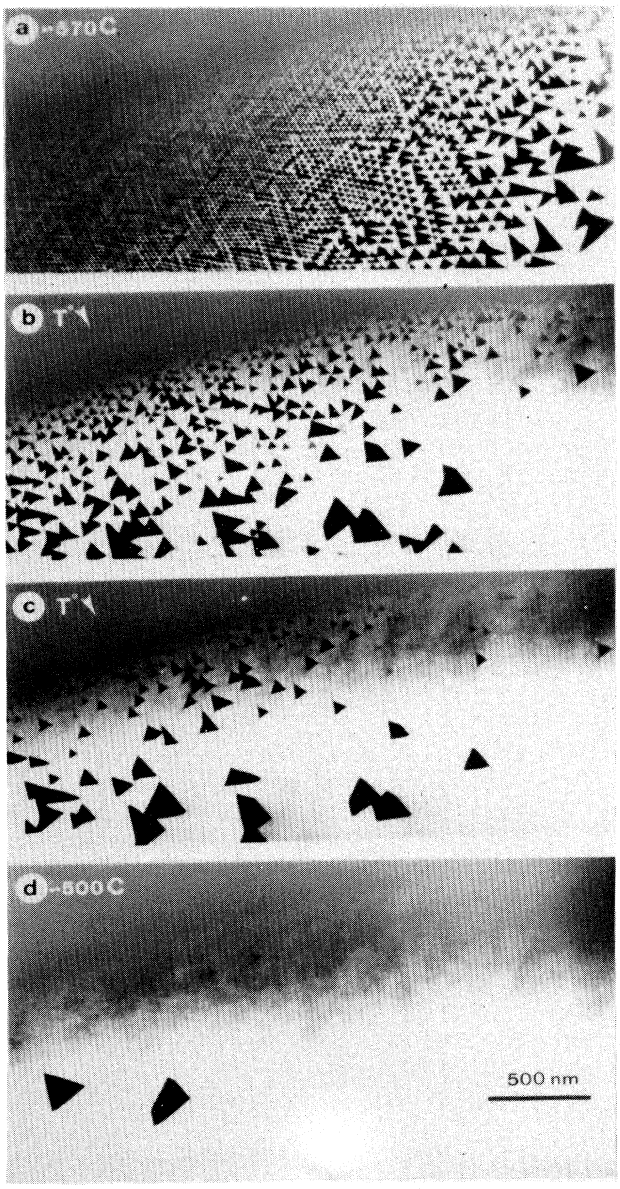

FIG. 11. Incommensurate phase "dissolving" on cooling.

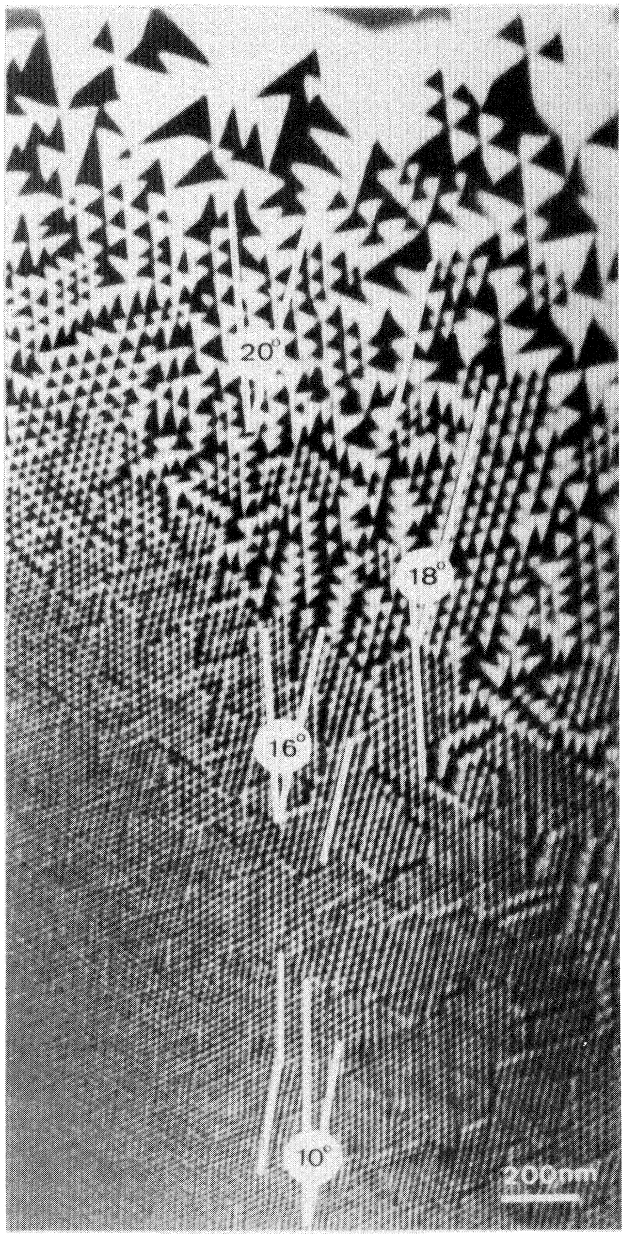

FIG. 12. Measurement of the angle 2ϵ as a function of temperature. The temperature difference between the top (cooler) and bottom (warmer) part of the figure is estimated to be about 5°.

be formed, one with the θ_+ walls of Fig. 4 (called a θ_+ macrodomain) and the other with the θ_- walls (called a θ_- macrodomain). The two different types of macrodomains are clearly identifiable in Fig. 8, and are seen to differ by a rotation of $\pi+2\epsilon$ (and not 2ϵ) about the **c** axis, in agreement with the prediction[5] of the model. Notice that a measurement of the difference in orientation of the rows of triangles in the two different macrodomains will determine the angle 2ϵ.

Neutrons can be diffracted from the regular triangular domain structure of the incommensurate phase (as well as from the underlying crystal lattice), thus producing satellites surrounding the normal α- or β-phase Bragg positions.[3,4] The magnitude of the satellite wave vectors is consistent with the triangular mesh size as determined by electron microscopy, although the accuracy of such a comparison is limited by a lack of accurate temperature determination in the electron microscopy experiments.[3] The neutron-diffraction experiments have not yet been able to determine the deviation of the satellite wave vectors from the a^* directions. The satellite wave vectors are perpendicular to the domain walls and thus each satellite peak observed by neutrons is in fact a superposition of two peaks with an angular separation of 2ϵ. Unfortunately, the neutron satellite peaks are relatively broad, probably as a result of the formation of relative small macrodomains; the angular width of a satellite peak can be es-

timated from the angular width of a hatched ellipsoid in Fig. 5 of the second of Refs. 4 and is approximately 20°. Since this is comparable with the largest of the values of 2ϵ determined here (see below) the observation of the splitting of the neutron satellites will be difficult, but perhaps not impossible assuming that the macrodomain structures in the samples used for neutron scattering are similar to those produced in the samples used for electron microscopy.

Optical diffraction of micrographs where the periodic array of Dauphiné columns is imaged as in Fig. 8 reveals satellites corresponding to the q vectors as shown in Figs. 9(a) and 9(b). This technique has sufficient resolution to observe the splitting of the satellites. If a single macrodomain is selected with a parallel laser beam, a diffraction pattern as in Fig. 9(a) is obtained revealing the triple-q satellites. Selecting an area across two macrodomains yields patterns as in Fig. 9(b), where the splitting of the satellites (angular separation 2ϵ) is clearly observed.

Splitting was also reported by Gouhara and Kato[9] who used a micro-Laue technique to reveal the satellites. The length of the q vector as well as the orientation characteristics are in good agreement with the direct-space evidence revealed by electron microscopy as will be further discussed below.

The macrodomain structure referred to in the discussion of Fig. 8 is also clearly observable in Fig. 10 where white lines separating different macrodomains have been inserted as an aid to the eye. Figure 10 shows the microstructure produced on heating from the α phase. One finds that on heating, rows of dagger-shaped triangles (each triangle having interior angles 2ϵ, 60°, and $120°-2\epsilon$) develop before the regular two-dimensional arrays of equilateral triangles develop; sometimes, instead of a row of dagger-shaped triangles, one finds a herringbonelike pattern (see Fig. 10). The regularity of these patterns is so striking that one is led to speculate that either a new phase is attempting to form as an intermediate phase between the α phase and the triangular incommensurate phase on warming, or that the observed patterns are formed because they are easier to nucleate than the triangular phase. This situation may be somewhat similar to that in $2H$-$TaSe_2$,[10] where a stripe phase is observed between the low-temperature commensurate phase and the double-honeycomb phase on heating, but not on cooling.

As can be seen in Fig. 11 there is no sign of regular arrays of dagger-shaped triangles on cooling. The triangular domain structure "dissolves" and isolated Dauphiné twins are left, the density of which decreases further with further decreasing temperature.

Figure 11 shows that the angle ϵ describing the deviation of the domain-wall orientation from a high-symmetry direction increases with decreasing temperature in agreement with the predictions of the phenomenological model as discussed above. In the lower-temperature region at the top of the figure where the triangles are relatively large, the individual domain-wall orientations are well defined and the boundaries narrow; consequently the angle 2ϵ can be determined by measuring the angle between two appropriately chosen domain walls. At higher temperatures, the angle 2ϵ can be obtained from a measurement of the relative orientation of the rows of triangles in two different macrodomains, as discussed in connection with Fig. 8. A variation in 2ϵ from 10° to 20° with decreasing temperature is indicated on the figure. Again this direct-space evidence agrees well with the results of Gouhara and Kato.[9]

In Figs. 8 to 12, where the individual Dauphiné twin domains are sufficiently large that the domain-wall orientation can be determined, the domain structures can be analyzed in terms of the six different domain walls shown in Fig. 4(a) and 4(b) as was done in Figs. 5 and 6. We have carried out such analyses of selected sections of Figs. 8 to 12, and in all cases found that the structures were well described in terms of these six domain walls.

Our conclusion is that the observed features of domain-wall geometry in both quartz and aluminum phosphate in the incommensurate phase, the α phase, and temperature region where the first-order incommensurate—to—α-phase transition is taking place, are understood both qualitatively and quantitatively in terms of the theoretical model.

ACKNOWLEDGMENTS

This work was supported by the Natural Sciences and Engineering Research Council of Canada.

*Also at Studie Centrum voor Kernenergie, B-2400, Mol, Belgium.

[1]G. Van Tendeloo, J. Van Landuyt, and S. Amelinckx, Phys. Status Solidi A **30**, K11 (1975).

[2]G. Van Tendeloo, J. Van Landuyt, and S. Amelinckx, Phys. Status Solidi A **33**, 723 (1976).

[3]G. Dolino, J. P. Bachheimer, B. Berge, C. M. E. Zeyen, G. Van Tendeloo, J. Van Landuyt, and S. Amelinckx, J. Phys. (Paris) **45**, 901 (1984).

[4]G. Dolino, J. P. Bachheimer, and C. M. E. Zeyen, Solid State Commun. **45**, 295 (1983); G. Dolino, J. P. Bachheimer, B. Berge, and C. M. E. Zeyen, J. Phys. (Paris) **45**, 361 (1984).

[5]M. B. Walker, Phys. Rev. B **28**, 6407 (1983).

[6]J. F. Scott, Rev. Mod. Phys. **46**, 83 (1974).

[7]G. Dolino and J. P. Bachheimer, Ferroelectrics **43**, 77 (1982).

[8]T. A. Aslanyan, A. P. Levanyuk, M. Vallade, and J. Lajzerowicz, J. Phys. C **16**, 6705 (1983).

[9]K. Gouhara and N. Kato, J. Phys. Soc. Jpn. **53**, 2177 (1984).

[10]R. M. Fleming, D. E. Moncton, D. B. McWhan, and F. J. DiSalvo, Phys. Rev. Lett. **45**, 576 (1980).

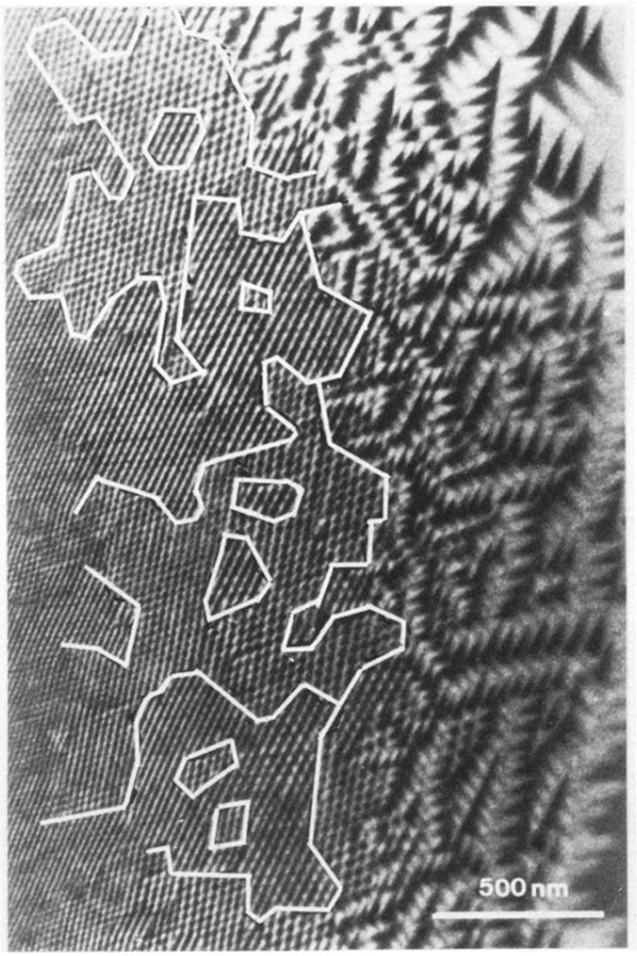

FIG. 10. Domain configuration obtained on heating from the α phase to the α-β transition temperature. A temperature gradient exists across the sample with the left of the figure being warmer than the right.

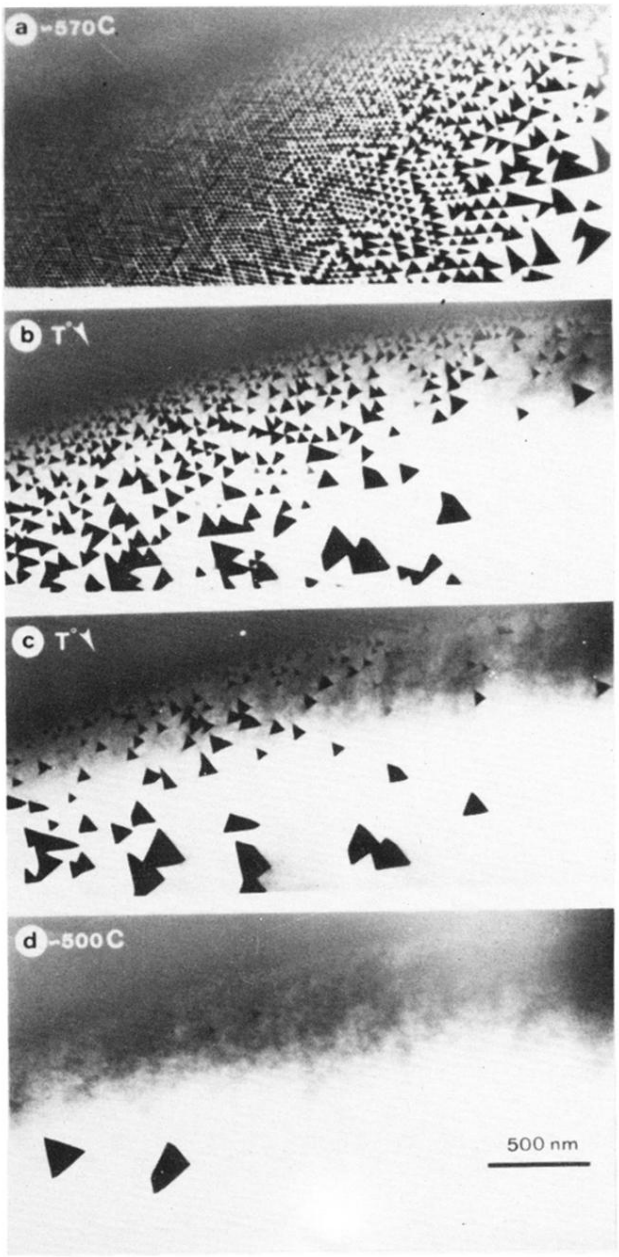

FIG. 11. Incommensurate phase "dissolving" on cooling.

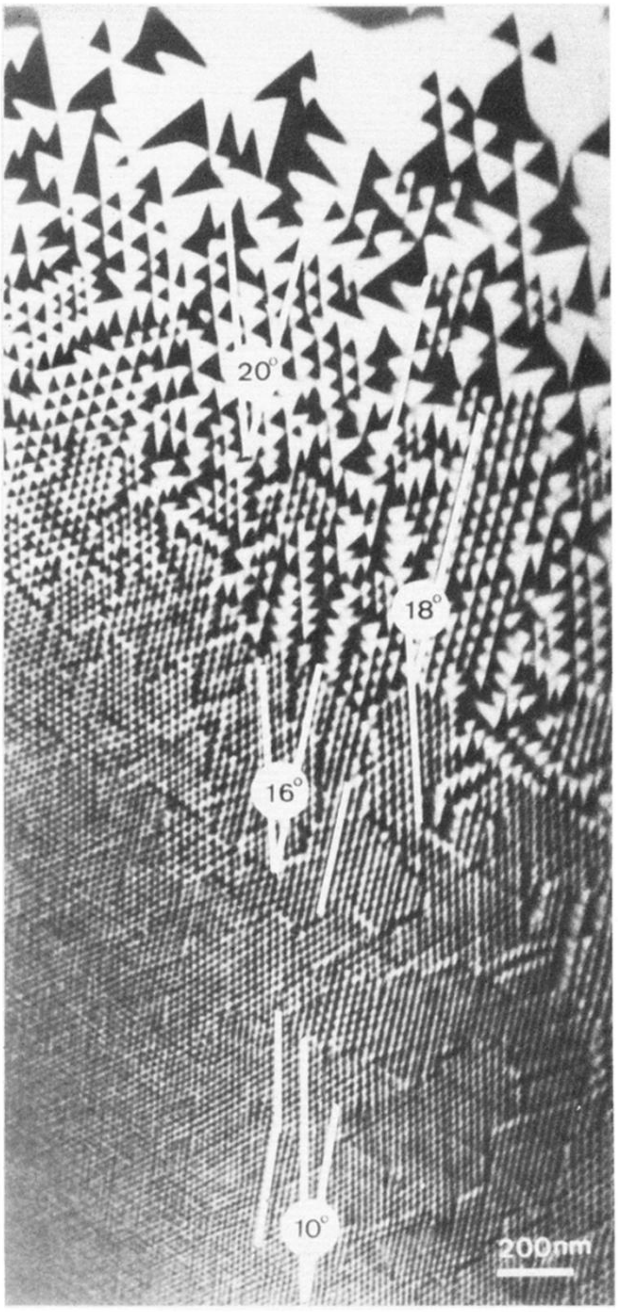

FIG. 12. Measurement of the angle 2ϵ as a function of temperature. The temperature difference between the top (cooler) and bottom (warmer) part of the figure is estimated to be about 5°.

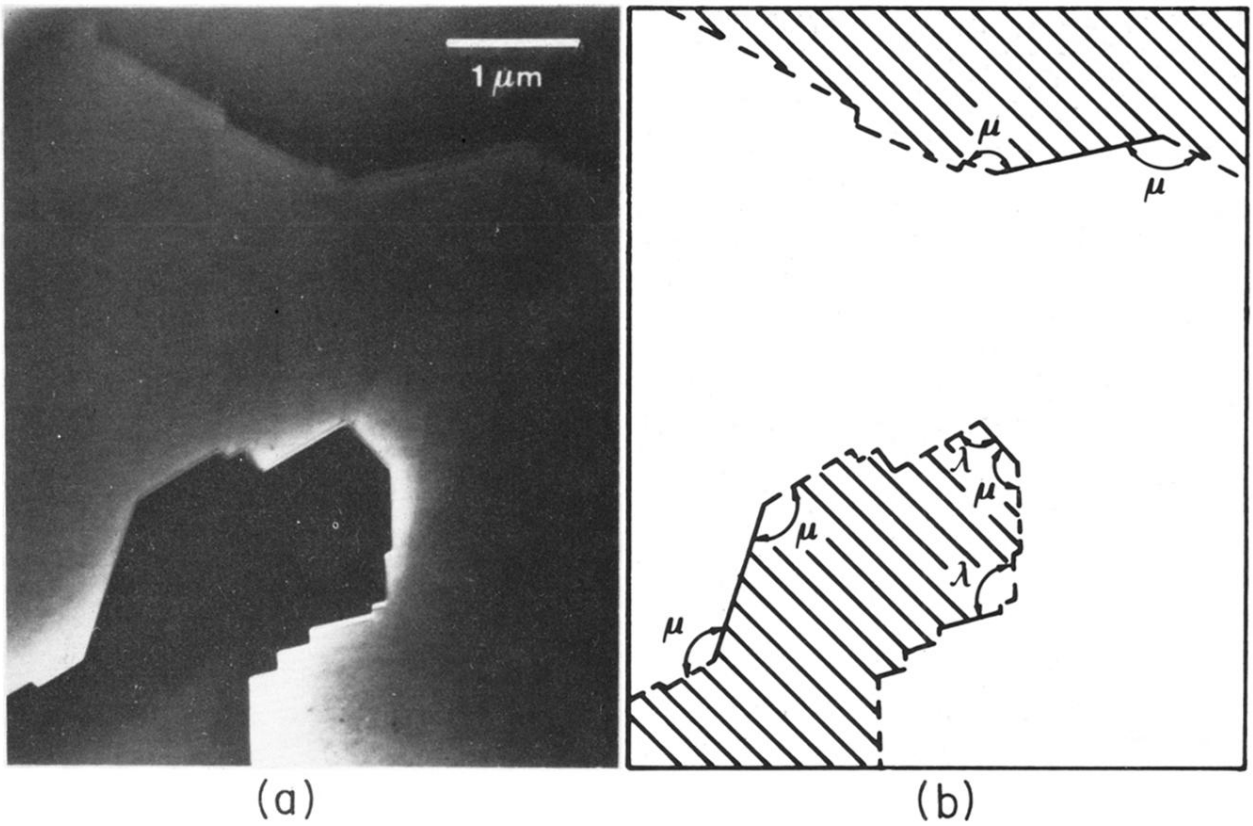

FIG. 5. (a) Dark-field image of coarse Dauphiné twins at room temperature in a foil of quartz, cut perpendicular to the **c** axis. (b) Analysis of the coarse domains of (a) in terms of the θ_+ and θ_- domain walls of Figs. 4(a) and 4(b); all of the labeled angles were measured, with the results $\lambda \simeq 101°$ and $\mu \simeq 139°$

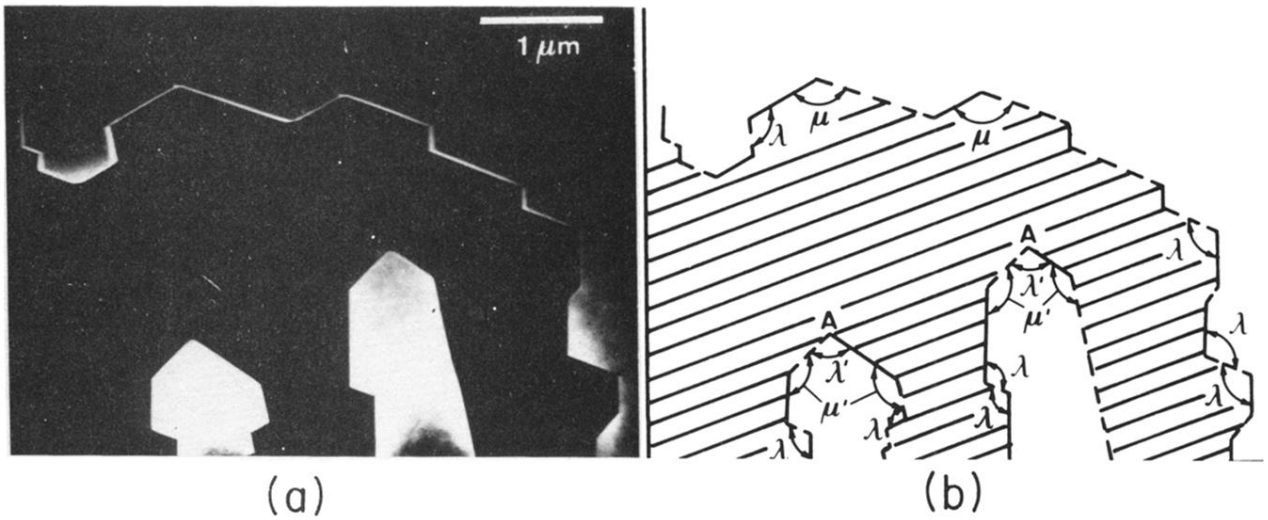

FIG. 6. (a) Dark-field image of coarse Dauphiné twins at room temperature in a foil of aluminum phosphate cut perpendicular to the **c** axis. (b) Analysis of the coarse domains of (a) in terms of the θ_+ and θ_- domain walls of Figs. 4(a) and 4(b); all of the labeled angles were measured, with the results $\lambda \simeq 110°$, $\mu \simeq 130°$, $\lambda' \simeq 100°$, and $\mu' \simeq 135°$.

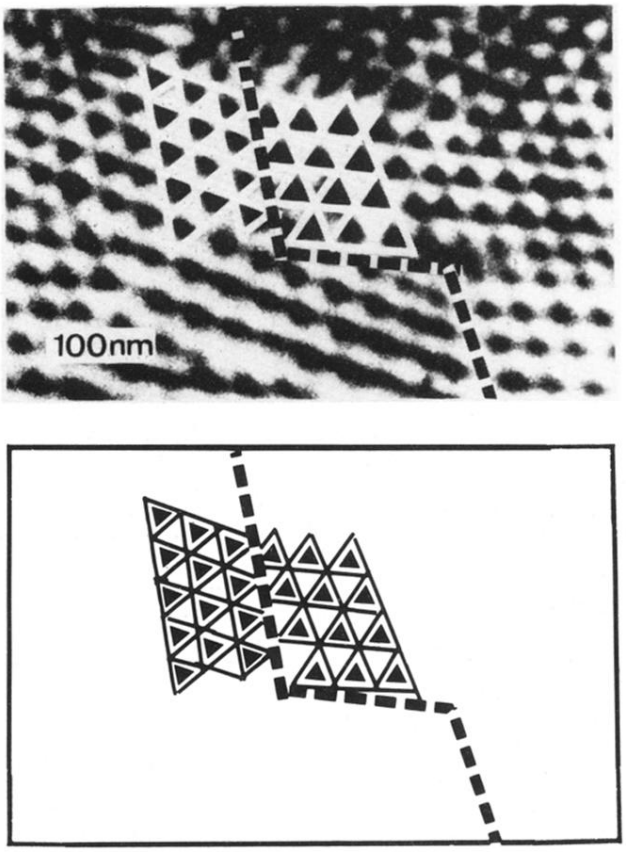

FIG. 8. An example of the triangular domain structure in quartz at a temperature of approximately $T = 846$ K showing two differently oriented macrodomains.

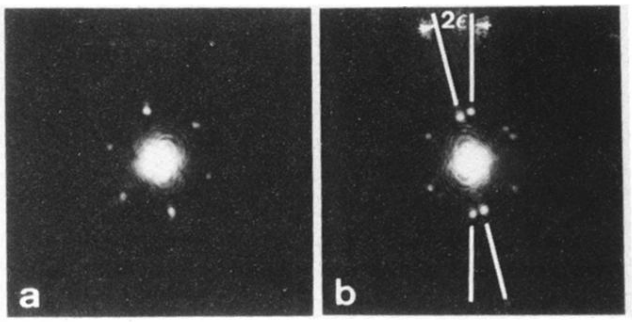

FIG. 9. Optical diffractographs of micrographs containing periodic arrays of Dauphiné twin columns. (a) Single macrodomain; (b) satellite splitting if area selected is across two macrodomains.